Three-body Coulomb description of pionic helium

Daniel Baye* and Jérémy Dohet-Eraly†
Physique Quantique and Physique Nucléaire Théorique et Physique Mathématique, C.P. 229, Université libre de Bruxelles (ULB), B-1050 Brussels, Belgium

(Received 15 December 2020; accepted 2 February 2021; published 17 February 2021)

The three-body Schrödinger equation of the system composed of an α particle He^{2+}, a negatively charged pion π^-, and an electron interacting through Coulomb forces is solved in perimetric coordinates with the Lagrange-mesh method. The ground state, quasibound states, and resonances are obtained for total orbital momenta $L = 0 - 20$. Mean distances between the particles allow for identifying the structure of these states. The widths of resonances broader than 10^{-5} atomic units are derived with the complex scaling method. A transition from atomic to molecular structure occurs between $L = 10$ and $L = 13$. Excited levels obtained for $L = 0 - 5$ display hydrogenlike properties for both the α-pion system and the electron excitations. Excited levels with $L \geqslant 14$ correspond to a vibrational excitation of the relative motion of the heavy particles. The validity of the Born-Oppenheimer approximation is found to be fair over the whole range of total orbital momenta.

DOI: 10.1103/PhysRevA.103.022823

I. INTRODUCTION

Spectroscopic measurements on systems interacting by the Coulomb force reach such a high precision that they can provide accurate information on the masses of the constituents. This method was successfully applied to the determination of the antiproton mass with studies of antiprotonic helium, a system composed of an α particle He^{2+}, an antiproton, and an electron. Such systems with long enough lifetimes are formed at high angular momenta when a beam of antiprotons impinges on helium [1]. They have been studied in very accurate spectroscopic experiments [1–3]. At these angular momenta, the three particles essentially interact through Coulomb forces and very accurate theoretical calculations are possible [4–8]. Together, experiment and theory provided a very precise measurement of the antiproton mass. Within the present experimental and theoretical error bars, this mass is found to be equal to the proton mass.

The same technique has been proposed to improve the value of the mass of the negatively charged pion π^- [9]. Recently, spectroscopic measurements on pionic helium composed of an α particle, a negative pion, and an electron have been performed [10]. A pion from a beam impinging on a superfluid helium target can replace an electron on its orbital and produce pionic helium π^4He^+ where the pion is excited, among others, to $n = 17$ hydrogenic orbitals. A transition induced by a tuned laser beam from the $L = 16$ level to the Auger-decaying $L = 15$ level is observed through the emitted products of π^- absorption by the ^{4}He nucleus. This promising result demonstrates the possibility of a future measurement of the pion mass with techniques of atomic spectroscopy.

A detailed theoretical knowledge of π^4He^+ is thus important. Following ideas of Condo [11], the first studies were performed by Russell [12–14]. Analysis of the three-body problem with the complex scaling method [15,16] can be found in Ref. [17]. Accurate calculations of the energies and widths of levels with high orbital momenta $L = 14 - 18$ are available in Ref. [9]. These long-lived levels correspond to transitions that might become accessible to experimental studies and Ref. [9] analyzes a possible experimental approach. As in the case of antiprotonic helium [8], our aim in the present paper is to study physical properties of pionic helium modeled as a nonrelativistic three-body system interacting through Coulomb forces, from its ground state to high angular momenta.

To this end, we use the Lagrange-mesh method [18–23] in the perimetric coordinate system [24,25]. This numerical method has the simplicity of a mesh calculation but its high accuracy is similar to the accuracy of a variational calculation. It does not require any analytical evaluation of matrix elements. Computer times are quite small. The method is found accurate in a variety of spectroscopic and collision applications [23]. For pionic helium, all states with an excited $\alpha\pi$ subsystem are unstable and the method consists of searching for stationary values of the energies. In the similar cases of antiprotonic helium [8] and antiproton-hydrogen systems [26], the accuracy on the energies matches or improves the best available results in the literature. Other properties of the system such as distances between particles can easily be computed [8,26]. The short computing times allow for performing a determination of the sensitivity of the energies to the pion mass. The Lagrange-mesh method can be combined with the complex scaling method [15,16] to provide energies and widths of resonances [23]. Calculations are then heavier since complex eigenvalues must be computed and found stationary with respect to the scaling parameter. The obtained widths describe the spontaneous dissociation of the system and are known as Auger widths.

The Lagrange-mesh method and the conditions of the numerical calculations are presented in Sec. II. Energies and

*dbaye@ulb.ac.be
†jdoheter@ulb.ac.be

mean distances between the different particles are given in Sec. III and the sensitivity to the value of the pion mass is analyzed in Sec. IV. Energies and widths of the broader resonances are computed with the complex scaling method in Sec. V. These results are discussed in Sec. VI and compared with the Born-Oppenheimer approximation. Section VII concludes with a summary. Atomic units (a.u.) are used throughout.

II. COMPUTATIONAL METHOD

A. Principle of Lagrange-mesh method in perimetric coordinates

We study the quantal three-body system formed by an α particle, a negatively charged pion, and an electron, interacting only through Coulomb forces. Fine structure and relativistic effects are not taken into account.

The Schrödinger equation is solved in perimetric coordinates to avoid numerical problems with the singularities of the kinetic-energy operator and of the Coulomb interactions. The system of perimetric coordinates [24,25] is composed of three Euler angles ψ, θ, ϕ defined on the basis of the heavy particles and the three dimensioned coordinates,

$$\begin{aligned} x &= r_{\alpha\pi} + r_{\alpha e} - r_{\pi e}, \\ y &= r_{\alpha\pi} - r_{\alpha e} + r_{\pi e}, \\ z &= -r_{\alpha\pi} + r_{\alpha e} + r_{\pi e}, \end{aligned} \tag{1}$$

involving the distances $r_{\alpha\pi}$, $r_{\alpha e}$, and $r_{\pi e}$ between the particles. The coordinates x, y, and z vary over the $(0, \infty)$ interval. In perimetric coordinates, the Coulomb potential reads

$$V(x, y, z) = -\frac{4}{x+y} - \frac{4}{x+z} + \frac{2}{y+z}. \tag{2}$$

The wave function with total orbital momentum L, projection M, and natural parity $(-1)^L$ is expanded as [22]

$$\Psi_M^L = \sum_{K=0}^{L} \mathcal{D}_{MK}^L(\psi, \theta, \phi)\Phi_K^L(x, y, z), \tag{3}$$

where the $\mathcal{D}_{MK}^L(\psi, \theta, \phi)$ with $K \geqslant 0$ are parity-projected and normalized Wigner angular functions [21]. In some cases, for $L > 0$, the sum over K can be truncated with excellent accuracy at some value $K_{\max}$. For $K_{\max} = 0$, the wave function presents a cylindrical symmetry along the $\alpha\pi$ axis. The value of $K_{\max}$ at convergence gives information about the departure from this symmetry.

Three definitions of the six perimetric coordinates are possible. They differ only through their angular coordinates. In each system, the three dimensioned coordinates are defined as in Eq. (1) up to a possible permutation. The choice used in this paper gives a special role to the two heavy particles. Their axis is close to the reference axis of the Euler angles. This allows for the use of small values for $K_{\max}$. For a limited number of excited states at low L, a faster and better convergence can, however, be obtained with the perimetric system where the reference particles are the ^{4}He nucleus and the electron. The results computed within this second perimetric system are followed by a star.

The $\Phi_K^L(x, y, z)$ functions in Eq. (3) are expanded in the Lagrange basis as

$$\Phi_K^L(x, y, z) = \sum_{i=1}^{N_x}\sum_{j=1}^{N_y}\sum_{k=1}^{N_z} C_{Kijk}^L F_{ijk}^K(x, y, z). \tag{4}$$

The definition and properties of the Lagrange functions F_{ijk}^K are given in Refs. [8,21,23]. Let us just mention that they are related to a three-dimensional mesh of $N_xN_yN_z$ points (h_xu_i, h_yv_j, h_zw_k), where u_i, v_j, w_k are the zeros of Laguerre polynomials of respective degrees N_x, N_y, N_z, and h_x, h_y, h_z are three scale parameters with the dimension of a length in atomic units. Each function F_{ijk}^K vanishes at all mesh points but the (ijk) one.

In the Lagrange-mesh method, all matrix elements are computed with the Gauss-Laguerre quadratures associated with the mesh. Hence, the matrix representing the kinetic energy has a block structure with elements expressed only with the zeros and weights of these quadratures [21,27]. The matrix representing the potential is diagonal with diagonal elements equal to the values of the potential at mesh points. The method thus involves searching a few eigenvalues (not necessarily the lowest ones) of a large sparse matrix. The eigenvalue calculations are performed with the software JADAMILU [28]. The search is performed in regions hinted from physics arguments or inspired by values of the literature.

It is important to realize that all states are unbound except for the ground state and its electronic excitations. Hence, the physically interesting eigenvalues may be embedded among eigenvalues corresponding to square-integrable approximations of states in the continuum. In this paper, the physical eigenvalues $E_{L\nu}$ are labeled by increasing order with the quantum number $\nu \geqslant 0$ and the unphysical ones are disregarded. Although unphysical eigenvalues are unstable when the condition of the calculation vary, their density may make the physical eigenvalues difficult to identify. Fortunately, two efficient signatures of physical states exist which must be consistently satisfied. At the Gauss approximation, the mean distances between α and π^- are given by

$$\langle r_{\alpha\pi} \rangle = \frac{1}{2}\sum_{Kijk} \left(C_{Kijk}^L\right)^2 (h_xu_i + h_yv_j) \tag{5}$$

and the probabilities of the K components by

$$P_L(K) = \sum_{ijk} \left(C_{Kijk}^L\right)^2. \tag{6}$$

At small L, the properties of physical eigenvalues resemble hydrogenic values as explained in Sec. VI A. At large L, unphysical eigenvalues are indicated by very large electron-α and electron-pion distances and probabilities of $K = 0$ indicating an unphysical structure.

Energies with few stable digits correspond to rather broad resonances. They can be better studied by combining the Lagrange-mesh method with the complex scaling method [15,16]. The coordinates x, y, z are then replaced by $e^{i\theta}x$, $e^{i\theta}y$, $e^{i\theta}z$, respectively, where θ is a real parameter. The complex-scaled Hamiltonian matrix for each L value is symmetric but not Hermitian. FEAST software [29,30] is used to compute the eigenvalues $E(\theta)$ of these sparse complex matrices. When

θ is varied, the real and imaginary parts of an eigenvalue stationary at θ_0,

$$E(\theta_0) = E_r - \tfrac{1}{2}i\Gamma, \tag{7}$$

provide approximations of the energy E_r and width Γ of a resonance.

B. Conditions of the numerical calculations

In atomic units, the mass of the α particle is chosen as $m_\alpha = 7294.29954142$, the mass of the negatively charged pion is chosen as $m_\pi = 273.13244$, and the mass of the electron is $m_e = 1$. The m_α/m_e ratio is taken from the CODATA 2018 recommended value [31]. The m_π/m_e ratio is deduced from the negative-pion mass 139.57039(18) MeV recommended by the Particle Data Group [32], which corresponds to $m_\pi = 273.13244(35)$ a.u.

For $L = 0$, the physical eigenvalues are obtained by searching for minima as in a variational calculation. For other L values, all states for which the $\alpha\pi$ system is excited are unbound and non-physical eigenvalues appear which require criteria of identification. For low L, the search can be guided by an approximation based on a double hydrogenic structure: the $\alpha + \pi^-$ and $\alpha\pi$ pseudoparticle + electron Coulomb systems. The approximate energies are [23]

$$E_L^{\rm app} = -\frac{m_\alpha m_\pi}{m_\alpha + m_\pi}\frac{2}{N^2} - \frac{(m_\alpha + m_\pi)m_e}{m_\alpha + m_\pi + m_e}\frac{1}{2n^2}, \tag{8}$$

where N and n are the respective hydrogenic principal quantum numbers of these systems. The search for $14 \leqslant L \leqslant 18$ can be guided by the accurate results of Ref. [9]. Other cases are based on the Born-Oppenheimer approximation (see Sec. VI D). The accuracy of the results is deduced from the stability of digits with respect to variations of all parameters.

The Lagrange-mesh basis depends on six parameters: the numbers of mesh points N_x, N_y, N_z and the scale parameters h_x, h_y, h_z. The search for optimal values of these parameters proceeds in several steps. First, the h_x, h_y, h_z parameter space is explored with the help of our experience with antiprotonic helium [8]. The parameters h_x and h_y should be close to each other and increase with the distance between the heavy particles. Parameters h_z should be in the vicinity of 0.4. Variations of these parameters with large enough numbers of mesh points lead to the roughly optimal values presented in Table I. The number of stable digits of the energies gives the best accuracy one can expect within the present approach. Then the numbers N_x, N_y, N_z of mesh points are reduced as long as this accuracy is not affected. Finally, the accuracy is checked by increasing these numbers by a few units.

The resulting choices of parameters are displayed in Table I. One observes that the stability of h_z in the vicinity of 0.4 is confirmed and that h_y becomes a little larger than h_x for $L \geqslant 12$. The behavior of the numbers of mesh points is similar to the one for antiprotonic helium. It is affected by the fact that the number of stable digits of the energies strongly decreases between $L = 5$ and 11. Up to $L = 14$, N_z is larger than the other two. For high L, N_y is the largest and all three decrease in spite of the fact that the number of stable digits increases as shown in Table II.

TABLE I. Optimal parameters for $K_{\rm max} = 2$. The same parameters are employed for $K_{\rm max} = 3$.

L	h_x	h_y	h_z	N_x	N_y	N_z
0	0.002	0.002	0.40	10	10	40
1	0.005	0.005	0.40	16	16	40
2	0.0035	0.0035	0.38	16	16	40
3	0.008	0.008	0.39	14	14	34
4	0.012	0.012	0.39	12	12	28
5	0.014	0.014	0.37	12	12	28
6	0.015	0.015	0.38	10	10	24
7	0.015	0.015	0.36	10	10	20
8	0.019	0.019	0.39	10	10	20
9	0.020	0.020	0.33	10	10	20
10	0.028	0.028	0.33	10	10	20
11	0.035	0.035	0.33	10	10	20
12	0.040	0.045	0.35	12	12	34
13	0.050	0.060	0.35	12	12	34
14	0.065	0.075	0.33	18	18	32
15	0.08	0.09	0.32	26	32	26
16	0.10	0.13	0.34	26	32	20
17	0.10	0.12	0.40	26	32	18
18	0.09	0.12	0.34	24	30	18
19	0.09	0.12	0.34	22	28	16
20	0.10	0.13	0.34	20	28	16

These parameters are used everywhere in this paper except for some $\nu \geqslant 2$ states with low L for which h_z had to be increased around 0.5 to obtain stable mean distances, and in some calculations with the second perimetric coordinate system.

In the complex scaling version of this method, the complex Hamiltonian matrix has the same structure with kinetic matrix elements multiplied by $e^{-2i\theta}$ and the potential matrix elements multiplied by $e^{-i\theta}$. The procedure starts with the optimal parameters of the real calculation. After slight adaptations of h_x, h_y, h_z, the parameter θ is varied and the numbers of mesh points are increased until convergence.

III. RESULTS

A. Energies and mean distances

In this section, we present the numerical properties of the results. Their physical contents are discussed later.

The energies $E_{L\nu}$ obtained with $K_{\rm max} = 2$ for $L \geqslant 2$ are displayed in Table II for the three lowest physical levels $\nu = 0$, 1, and 2 for each $\alpha\pi$ excitation. Nonphysical eigenvalues, i.e., which are not stable with respect to variations of the parameters, are disregarded. The identification of unstable eigenvalues is made easy by the verification of the two criteria mentioned in Sec. II B. For $L = 1$ and 2, the second row presents physical energies for $\nu \geqslant 3$.

The displayed digits are stable with respect to variations of the numbers of points and scale parameters, except the last one which may vary by a few units. Within the given accuracy, the results with $K_{\rm max} = 3$ are identical to those with $K_{\rm max} = 2$ while the results with $K_{\rm max} = 1$ are identical up to $L = 14$ and less accurate beyond.

TABLE II. Energies $E_{L\nu}$ obtained with $K_{\max} = 2$ for $\nu = 0$, 1, and 2. For $L = 1$ and 2, the second row presents energies for $\nu \geqslant 3$. All the displayed digits are stable with respect to variations of the numbers of points and scale parameters, except the last one which may vary by a few units. The results computed within the second perimetric coordinate system are followed by a star.

L	E_{L0}	E_{L1}	E_{L2}
0	−527.048402397489	−526.6734454321	−526.6040093
1	−132.1371354	−131.76210948	−131.76209874*
	−131.692667	−131.692663*	
2	−59.00576	−58.630423	−58.63037*
	−58.56095	−58.56094*	−58.561
3	−33.41052	−33.03443	−33.0342*
4	−21.5648	−21.187	−21.187
5	−15.132	−14.752	−14.75
6	−11.256		
7	−8.745		
8	−7.03		
9	−5.81		
10	−4.91		
11	−4.243		
12	−3.7420		
13	−3.35846		
14	−3.05695	−2.8586	
15	−2.828551836	−2.6854268	−2.580022
16	−2.65751436078	−2.556986432	−2.48154177
17	−2.531948046652	−2.461807966154	−2.40704312870
18	−2.441386916525	−2.3911785509990	−2.35006537007
19	−2.3761071558417	−2.3381714951671	−2.3059519455157
20	−2.3278801636876	−2.2975736468200	−2.2712868515908

The number of stable digits for $\nu = 0$ strongly varies with L. The stable ground-state energy (of the Coulomb three-body system) has 12 decimal digits, i.e., a relative accuracy better than 10^{-14}. The $L = 1$ energy $E_{1,0}$ has seven stable decimal digits. This indicates a narrow level. For $L \geqslant 2$, the number of stable digits continues to decrease and reaches a minimum for $8 \leqslant L \leqslant 10$. From $L = 5$ to $L = 11$, the resonances should be broad. Physical energies of excited levels could not be found among the eigenvalues for $6 \leqslant L \leqslant 13$.

The number of stable digits increases beyond $L = 12$. Excited levels become again identifiable for $L \geqslant 14$. Very different parameter choices are possible for $L = 14$ (and to a lesser extent for $L = 16$). The number of stable digits becomes large at $L = 15$ and continues to increase beyond. The levels with $L > 15$ are very narrow and correspond to quasibound states as shown by their narrow widths in Ref. [9].

The mean distances $\langle r_{\alpha\pi}\rangle$, $\langle r_{\alpha e}\rangle$, and $\langle r_{\pi e}\rangle$ are presented in Table III for the levels of the energies shown in Table II. Here also the displayed digits are stable with respect to variations of the numbers of points and scale parameters, except the last one which may vary by a few units. For high L, the number of decimal digits has been limited to nine.

As expected from the centrifugal effect, the mean distance between α and π^- increases with L. For $\nu = 0$, $\langle r_{\alpha e}\rangle$ is close to 1.5 for low L and then progressively decreases with, however, a fluctuation between $L = 9$ and 12. This fluctuation corresponds to energies with very few stable digits. Because of the repulsion between pion and electron, $\langle r_{\pi e}\rangle$ is always larger than $\langle r_{\alpha e}\rangle$. The difference is significant for the quasibound levels with $L \geqslant 14$ for which $\langle r_{\alpha\pi}\rangle$ indicates a moleculelike structure.

IV. SENSITIVITY TO THE PION MASS

The energies in Table II are computed with the 2020 value of the pion mass $m_{20} = 273.13244$ a.u. This value is given with an error 0.00035. If a new measurement improves this mass or if spectroscopic data for $\pi^4\mathrm{He}^+$ become available, the corresponding energies can be obtained with the first-order approximation:

$$E_{L\nu}(m_\pi) = E_{L\nu}(m_{20}) + \frac{\Delta E_{L\nu}}{\Delta m_\pi}(m_\pi - m_{20}). \tag{9}$$

The coefficients $\Delta E_{L\nu}/\Delta m_\pi$ are given in Table IV for levels the energy of which is accurate enough to be sensitive to the pion mass. These coefficients are computed with energy differences $\Delta E_{L\nu}$ corresponding to $\Delta m_\pi = 0.0001$ around $m_{20} = 273.13244$. They are stable over the interval $[273.1321, 273.1328]$ which covers the experimental error interval. The accuracy of energies obtained with Eq. (9) is equivalent to the accuracy in Table II within at least this interval.

The sensitivity coefficients can also be computed using the Hellmann-Feynman theorem. The Lagrange-mesh matrix elements of the derivative of the kinetic energy operator with respect to the pion mass are obtained by differentiating Eqs. (A.2) and (A.3) of Ref. [22] with respect to m_π. The obtained values for $dE_{L\nu}/dm_\pi$ are identical to those displayed in Table IV except for two cases of different rounding of the last displayed digit.

For low L, the correction is almost independent of ν. For high L, the sensitivity to the pion mass decreases when ν increases.

TABLE III. Mean distances for the states of the energies shown in Table II. The results computed within the second perimetric coordinate system are followed by a star.

L	ν	$\langle r_{\alpha\pi}\rangle$	$\langle r_{\alpha e}\rangle$	$\langle r_{\pi e}\rangle$
0	0	0.002848741	1.500175901	1.500179275
	1	0.002848741	6.0007479	6.0007487
	2	0.002848741	13.501	13.501
1	0	0.009495811	1.49994	1.49998
	1	0.009495803	6.000279	6.000287
	2	0.011394931*	5.0006603*	5.0006727*
	3	0.009495802	13.502	13.502
	4	0.01139494*	12.50157*	12.50158*
2	0	0.0199416	1.49893	1.49918
	1	0.0199413	5.9982	5.9982
	2	0.0237394*	5.00071*	5.00084*
	3	0.019941	13.50	13.50
	4	0.02374*	12.51*	12.51*
	5	0.019941	10.72	10.72
3	0	0.034187	1.496	1.497
	1	0.034185	5.992	5.993
	2	0.039882*	5.02*	5.02*
4	0	0.052235	1.492	1.493
	1	0.05225	5.98	5.98
	2	0.0597	5.02	5.02
5	0	0.07408	1.486	1.489
	1	0.07408	5.96	5.97
	2	0.0835	5.01	5.01
6	0	0.09973	1.48	1.49
7	0	0.1292	1.48	1.49
8	0	0.1625	1.51	1.53
9	0	0.1998	1.56	1.58
10	0	0.241	1.75	1.79
11	0	0.284	3.53	3.56
12	0	0.3287	3.33	3.40
13	0	0.4075	1.24	1.40
14	0	0.4848	1.115	1.312
	1	0.6055	1.138	1.420
15	0	0.57664067	1.0350657	1.2905909
	1	0.73042857	0.9653385	1.3338381
	2	0.90483647	0.9151283	1.4181488
16	0	0.69073016	0.96432048	1.29923273
	1	0.87326247	0.90515545	1.38020919
	2	1.07264575	0.86456954	1.49973260
17	0	0.834453038	0.901076730	1.342403542
	1	1.043295417	0.859051990	1.467555526
	2	1.261884071	0.831930767	1.622767765
18	0	1.010866577	0.849770272	1.428203899
	1	1.237343804	0.824372959	1.59154337
	2	1.469325228	0.807876261	1.77533156
19	0	1.212783428	0.813259477	1.555235109
	1	1.448460480	0.799656222	1.745395412
	2	1.690329100	0.790224113	1.951044740
20	0	1.426659641	0.789936883	1.711433369
	1	1.669218577	0.782885259	1.920624110
	2	1.920261120	0.777607436	2.144011718

The energies presented in Ref. [9] are computed with a different pion mass but also with a different mass of the α particle. In Table V, we display the results of the present calculation performed with the CODATA 2012 value $m_{\rm He} = 7294.2995361$, and the rounded mass $m_\pi = 273.132$. These energies are compared with those of Refs. [9,33]. The agreement is excellent for $L = 17$ and 18 and reasonable for the other ones.

TABLE IV. Numerical derivatives $\Delta E_{L\nu}/\Delta m_\pi$ of the energies $E_{L\nu}$ with respect to the pion mass.

L	$\nu = 0$	$\nu = 1$	$\nu = 2$
0	−1.8582328	−1.8582328	−1.8582328
1	−0.4645576	−0.4645581	−0.4645582
2	−0.2064674		−0.2064700
3	−0.11614		
14	−0.006897	−0.00564	
15	−0.00554852	−0.0043810	−0.003499
16	−0.00436867	−0.00343706	−0.00277239
17	−0.00335686	−0.00268279	−0.00221817
18	−0.00254392	−0.00210535	−0.00179436
19	−0.00194906	−0.00167763	−0.00147024
20	−0.00154337	−0.00136818	−0.00122453

With Eq. (9) and Table IV, the energies of Table II can be updated if a new value of the pion mass is recommended. They can also be used to derive such a mass from future spectroscopic data. The fine-structure corrections depend on the pion mass through the three-body wave functions. The corrections given in Table I of Ref. [9] should remain valid for an accuracy around $10^{-9} - 10^{-10}$ on the energies.

V. COMPLEX SCALING

In this section, we study the properties of the resonances with the complex scaling method. This method is numerically heavier since matrices are both complex and larger but provides resonance energies and widths. These Auger widths are decay widths of the system, i.e., widths for the decomposition into a system $\alpha\pi$ and an electron. Electromagnetic widths require a separate calculation which is not performed here. It is shown in Ref. [9] that electromagnetic transitions are not the main decay process.

The energies $E_{L0}^{\rm CS}$ and widths Γ_{L0} of levels broader than 10^{-5} are computed with the complex scaling method and presented in Table VI. They are compared with the stationary energies E_{L0} of Table II. These energies and the corresponding parameters are good starting points for the search of stationary eigenvalues in the complex scaling method. The values of the scale parameters h_x, h_y, h_z are identical or close to those of Table I. Between $L = 3$ and 11, $N_x = N_y$ are increased to 16 or 18 and N_z is in the range $30 - 36$. For $L = 12$, we could not find stable results with $K_{\rm max} > 1$. Values $N_x = N_y = 20$ and $N_z = 44$ are used for $L = 13$ and 14.

The resonance energies are obtained with five to six stable decimal digits between $L = 2$ and 10. As before, an error of a few units may affect the last displayed decimal digit. Simultaneously, the widths progressively increase from about 10^{-5} to about 0.01. At $L = 11$, the accuracy drops. This is not surprising. The mean electron distances are very large for $L = 11$ and 12 in Table III, indicating a wave function poorly approximated by square-integrable functions. The complex

TABLE V. Comparison of present energies E_{Lv} (first rows) computed for $m_{\mathrm{He}} = 7294.2995361$ and $m_\pi = 273.132$ with those of Refs. [9,33] (second rows).

L	E_{L0}	E_{L1}	E_{L2}
14	−3.0569483	−2.858595	
	−3.0569481417(4)	−2.858617029(2)	−2.70984178(2)
15	−2.8285493943	−2.6854249	−2.580020
	−2.82854939373(4)	−2.68542722(2)	−2.58002554(1)
16	−2.65751243855	−2.5569849200	−2.48154055
	−2.65751243850171	−2.556984919572(2)	−2.481540552377(5)
17	−2.531946569606	−2.461806785706	
	−2.5319465695913	−2.4618067856861	
18	−2.4413857971811	−2.3911776246295	
	−2.4413857971745		

scaling method would probably require a much more extended basis to improve the accuracy. The same comment is valid for $L = 12$. At $L = 13$, the width becomes much smaller and the energy again displays six stable decimal digits. The $L = 14$ energy and width are confirmed by the more accurate results of Ref. [9], after correcting the energy with the help of Table IV. Beyond $L = 14$, the widths become too small to be obtained with the present set of coordinates. Those larger than 10^{-10} are derived in Ref. [9] for $L = 14 - 16$.

The resonance energies E_{L0}^{CS} fairly agree with the stationary values E_{L0} and the widths explain the number of stable digits of E_{L0} that could be found. There is an excellent correlation between this number obtained independently and the widths Γ_{L0}.

VI. DISCUSSION

A. $L = 0 - 5$

The ground-state energy in Table II is well reproduced by the approximation (8), with an error smaller than 10^{-5} a.u. This approximation corresponds to a $1s$ electron orbiting a charge $+1$ with mass $m_\alpha + m_\pi$ and the $\alpha + \pi^-$ system in a $1S$ hydrogenic ground state. The corresponding Bohr radii are denoted as $a_{\alpha\pi}$ and $a_{(\alpha\pi)e}$, respectively. The mean distance $\langle r_{\alpha\pi}\rangle$ presented in Table III does not differ from the hydrogenic value $1.5a_{\alpha\pi}$ with $a_{\alpha\pi} = 0.0018991604$. The mean distances $\langle r_{\alpha e}\rangle$ and $\langle r_{\pi e}\rangle$ are close to the hydrogenic value $1.5a_{(\alpha\pi)e} = 1.500198218$ with $a_{(\alpha\pi)e} = 1.0001321452$.

For $L = 0$, K is equal to zero. All states present an axial symmetry around an axis close to the $\alpha\pi$ axis. The first two excited states correspond to $2s$ and $3s$ excitations of the electron around the $\alpha\pi$ system in its ground state as shown by the unmodified value of $\langle r_{\alpha\pi}\rangle$. Their excitation energies shown in Table VII closely reproduce the corresponding hydrogenic energies displayed in the last row. Their mean distances $\langle r_{\alpha e}\rangle$ and $\langle r_{\pi e}\rangle$ do not deviate much from the mean distances $6a_{(\alpha\pi)e}$ and $13.5\,a_{(\alpha\pi)e}$ given by the expression

$$\langle r\rangle_{nl} = \tfrac{1}{2}[3n^2 - l(l+1)]a_{(\alpha\pi)e} \tag{10}$$

of an hydrogenic state nl.

The lowest $L = 1$ states correspond to the $2p$ and $3p$ electron excitations around the $1S$ $\alpha\pi$ state. These states are not found with the first coordinate system under the conditions of Table I because the angular part in Eq. (3) is not appropriate for an electron np orbital. They are easily obtained with the second system as explained in Sec. II A. The $2p$ level is about 10^{-6} a.u. above the $2s$ level and the $3p$ level is even closer to the $3s$ level. In the following, we shall focus on levels corresponding to excitations of the $\alpha\pi$ subsystem.

The $L = 1$ lowest state presented in Table II closely corresponds to a $1s$ electron orbiting the $\alpha\pi$ subsystem in a $2P$ excited state. The value of $\langle r_{\alpha\pi}\rangle$ is close to $5a_{\alpha\pi} = 0.009495802$. The excited $L = 1$ states essentially have an

TABLE VI. Energies E_{L0}^{CS} and widths Γ_{L0} from complex scaling. Comparison with the static energies E_{L0} of Table II.

L	E_{L0}^{CS}	Γ_{L0}	E_{L0}
2	−59.00576	1.3[−5]	−59.00568
3	−33.410476	8.6[−5]	−33.4104
4	−21.564793	3.32[−4]	−21.5648
5	−15.132146	9.09[−4]	−15.132
6	−11.256501	2.004[−3]	−11.256
7	−8.745336	3.794[−3]	−8.745
8	−7.029467	6.395[−3]	−7.03
9	−5.809676	9.785[−3]	−5.81
10	−4.916784	1.368[−2]	−4.91
11	−4.2496	1.74[−2]	−4.243
12			−3.7420
13	−3.358486	5.7[−5]	−3.35846
14	−3.056951	1[−5]	−3.05695

TABLE VII. Energy differences $E_{Lv} - E_{L0}$ for $L = 0 - 3$ presented as a function of the hydrogenic quantum numbers nl. The final row presents the excitation energies of an electron orbiting a system with the total mass of α and π^-. The hydrogenic ground-state energy is −0.499933936 a.u. The results computed within the second perimetric coordinate system are followed by a star.

L	$2s$	$2p$	$3s$	$3p$	$3d$
0	0.37496		0.44439		
1	0.37503	0.37504*	0.44447	0.44447*	
2	0.37534	0.37539*	0.44481	0.44482*	0.4448
3	0.37609	0.3763*	0.4456		
$(\alpha\pi)e$	0.37495	0.37495	0.44439	0.44439	0.44439

axial symmetry with only a 10^{-7} probability of the $K = 1$ component. Their approximate structure is $(NL_{\alpha\pi}, nl) = (2P, ns)$ as shown by their energies and mean distances. The $(2S, np)$ levels are obtained only with the second coordinate system. They lie a little above the corresponding $(2P, ns)$ levels. The $\alpha\pi$ mean distance is 0.01139493 for the $(2S, 2p)$ state in agreement with $6a_{\alpha\pi} = 0.01139496$ and close to that value for the $(2S, 3p)$ state. The other mean distances are consistent with the expected values of an excited $2p$ or $3p$ electron.

For $L = 2$, the structure becomes more complicated with $K_{\max} = 2$. The search for optimal parameters was more difficult. The first five excited levels could be studied with various accuracies. Their energies are given in Table II and their excitation energies with respect to $\nu = 0$ in Table VII. All six states have approximate $(NL_{\alpha\pi}, nl)$ hydrogenic properties with $L_{\alpha\pi}$ and l coupled to L. The $\nu = 0$ state has a distance $\langle r_{\alpha\pi}\rangle$ close to the $3D$ mean distance $10.5a_{\alpha\pi} = 0.1994118$ like the $\nu = 1$, 3, and 5 ones. For the $\nu = 2$ and 4 states, this distance is similar to the $3P$ distance $12.5a_{\alpha\pi} = 0.0237395$. The order of the levels is $(3D, 1s)$, $(3D, 2s)$, $(3P, 2p)$, $(3D, 3s)$, $(3P, 3p)$. The location of $(3D, 3d)$ is uncertain because the energy is not precise enough. The identification of the quantum numbers is easy with the mean distances of Table III. The $3d$ mean distance starts to differ from the hydrogenic mean distance $10.5\, a_{(\alpha\pi)e}$. While ns states are dominantly $K = 0$ with $K = 1$ and 2 probabilities smaller than 3×10^{-5} and 10^{-7}, respectively, other states have more complicated structures to comply with the coupling schemes necessary for a total orbital momentum $L = 2$.

A few levels are clearly identified among unphysical eigenvalues for $L = 3 - 5$. They correspond to $(NL_{\alpha\pi}, 1s)$, $(NL_{\alpha\pi}, 2s)$, and $(NL_{\alpha\pi}, 2p)$ with $N = L_{\alpha\pi} + 1$ in the hydrogenic approximation. The mean distances still follow Eq. (10) but less precisely. The widths of these levels increase when L increases, in parallel with the decrease of the number of stable digits of the three-body energies.

B. $L = 6 - 13$

From $L = 6$ to $L = 12$, only one stationary solution could be found, with few stable digits. This corresponds to widths larger than 10^{-3} a.u. in Table VI. For $L \leqslant 9$, the energies and mean distances still resemble hydrogenic values, but not accurately. For $L = 10 - 12$, the mean distances between the electron and the heavy particles increase strongly. The dissociation widths exceed 0.01 for $L = 10$ and 11. In these cases, the corresponding square-integrable wave functions are very poor approximations of complicated scattering wave functions. The probabilities $P_L(1)$ become larger than 13% for $L = 11$ and 12, and the probabilities $P_L(2)$ and $P_L(3)$ are far from negligible. The bound-state approximation is very poor here but the stationary energies are still not far from the resonance energies given by the complex scaling.

The results for $L = 13$ indicate the start of a significant change. The mean distances $\langle r_{\alpha e}\rangle$ and $\langle r_{\pi e}\rangle$ suddenly drop while $\langle r_{\alpha\pi}\rangle$ continues to increase steadily to reach about 0.5 a.u. The probability $P_L(0)$ jumps from 0.84 to 0.98 from $L = 12$ to $L = 13$. A transition occurs to a pseudomolecular structure. No excited state could be found.

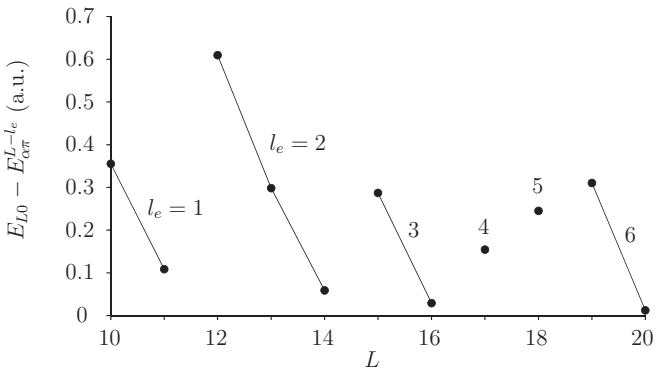

FIG. 1. Electron emission energy $E_{L0} - E_{\alpha\pi}^{L-l_e}$ for the lowest electron orbital momentum l_e as a function of L, where $E_{\alpha\pi}^{L-l_e}$ is the energy of the highest open threshold below E_{L0}.

C. $L = 14 - 20$

The states with $L \geqslant 14$ present a molecular structure in spite of the fact that the heavy particles attract each other because the distance between them is made large by the centrifugal effect. Moreover, their dissociation widths start to decrease very fast when L increases. Widths for $L = 14 - 16$ are given in Ref. [9]. For higher L values, the widths were too small to be computed. The reason of this decrease is well known [1,11]: the spontaneous dissociation by emission of an Auger electron is hindered because the orbital momentum l_e of the emitted electron increases.

This effect is illustrated in Fig. 1. The electron emission energy $E_{L0} - E_{\alpha\pi}^{L-l_e}$ for the lowest orbital momentum l_e is computed as a function of L with respect to the closest open threshold $E_{\alpha\pi}^{L-l_e}$. The values are labeled l_e. This orbital momentum increases from 1 to 2 at $L = 12$. It is still equal to 2 at $L = 14$ but the emission energy drops. The dissociation width of the $L = 14$ level is about 10^{-5} [9], not yet very small. At $L = 15$, l_e becomes equal to 3 and the width drops to 4×10^{-10}. The stationary energy $E_{15,0}$ has nine stable digits. Beyond $L = 16$, l_e continues to increase. The widths become very small, smaller than 10^{-13} for $\nu = 0$. The pseudomolecular levels are quasibound. The main decay channel is the pion decay $\pi^- \to \mu^- + \nu_\mu$ rather than radiative [9].

For $L \geqslant 15$, the pseudomolecule adopts a near axial structure. The probabilities $P_L(3)$ and $P_L(2)$ become negligible for $L \geqslant 16$ and $L \geqslant 18$, respectively. The mean distance between α and π^- increases with L and with the vibrational excitation. Simultaneously, the mean distance between the α particle and the electron decreases when L or ν increases as the screening by the pion become weaker, while the pion-electron distance increases. The pseudomolecule progressively takes a polar form.

D. Comparison with Born-Oppenheimer approximation

The Born-Oppenheimer approximation is efficient in molecular systems involving two heavy particles. The present system is different from a molecule by the fact that the heavy particles attract each other. Nevertheless, at large distances between the particles, the effect of this difference should be weak and the approximation should be valid. Here we explore

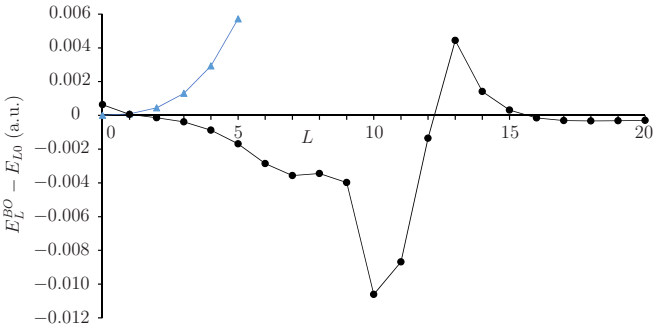

FIG. 2. Differences of the energies $E_L^{\rm BO}$ computed at the Born-Oppenheimer approximation and the three-body energies E_{L0} of Table II for $L = 0 - 20$ (black dots). Differences $E_L^{\rm app} - E_{L0}$ are also displayed as blue triangles.

its validity for a large range of distances between the heavy particles.

The Born-Oppenheimer equation for the electron reads

$$\left(-\frac{1}{2}\Delta - \frac{2}{r_{\alpha e}} + \frac{1}{r_{\pi e}} - \frac{2}{R}\right)\chi(\boldsymbol{r}_{\alpha e}, R) = \mathcal{E}(R)\chi(\boldsymbol{r}_{\alpha e}, R), \tag{11}$$

where $R \equiv r_{\alpha\pi}$ is fixed and the Laplacian Δ corresponds to the α-electron coordinate $\boldsymbol{r}_{\alpha e}$. The ground-state energy $\mathcal{E}(R)$ depends on the parameter R. It is computed in confocal elliptic coordinates (or prolate spheroidal coordinates) [34] with the Lagrange-mesh method as explained in Ref. [35]. A Lagrange-Laguerre mesh with 20 points is employed for the coordinate $(r_{\alpha e} + r_{\pi e})/R - 1$. The mesh is scaled with a parameter $h = 0.5/R$ for $R < 0.002$, $0.4/R$ for $0.002 \leqslant R < 0.02$, and $0.35/R$ for $R \geqslant 0.02$. These values belong to the plateaus of optimality for each R value. A Lagrange-Legendre mesh with ten points is used for the coordinate $(r_{\alpha e} - r_{\pi e})/R$.

The energies $\mathcal{E}(R)$ become a potential for the next step of the procedure. The radial Schrödinger equation of partial wave L with this potential is solved on a regularized Laguerre mesh with 20 points for R scaled with a parameter h_L. The zeros of this regularized mesh are identical to those of the non-regularized Laguerre mesh used for the solution of Eq. (11); both mesh methods differ only by the matrix elements of the kinetic energy (see Sec. 3.3.4 of Ref. [23] with $\alpha = 0$). After a search for optimal values belonging to plateaus of stability of the lowest Born-Oppenheimer energies $E_L^{\rm BO}$, the scale parameter h_L is parametrized as a function of $L > 0$ as $h_L = 0.0012\,L + 10^{-7}\,L^4$. For $L = 0$, we use $h_0 = 0.0012$. With these choices, the energies $E_L^{\rm BO}$ have an accuracy of about 10^{-10} with respect to variations of h, h_L, and the three numbers of mesh points.

The differences between the Born-Oppenheimer energies $E_L^{\rm BO}$ and the three-body energies E_{L0} of Table II are displayed as black dots in Fig. 2. Differences involving the approximate energies $E_L^{\rm app}$ defined in Eq. (8) are also displayed as blue triangles for low L values. The Born-Oppenheimer approximation is better than the hydrogenic approximation except for $L = 0$. It is very good for $L \geqslant 14$, as expected, but also fair for $L \leqslant 9$ and $L = 13$. The sign of the difference varies in the different ranges. For $L = 10 - 13$, the approximation is significantly less good, except accidentally for $L = 12$, but can still be a useful guide for a search of three-body resonances.

VII. SUMMARY

To summarize, the $\pi\mathrm{He}^-$ pionic helium described with Coulomb forces has been studied with the three-body Schrödinger equation in perimetric coordinates with the Lagrange-mesh method. Energies of bound, quasibound, and resonant states are obtained for $L = 0$ to 20. Calculations are simple and fast once optimal values for the various parameters are established. Except when the $\alpha\pi$ subsystem is in its ground state, all states are unbound resonances with a large variety of properties. The energies and widths of these resonances are derived for $L = 2 - 14$ with the complex scaling method. For these L values, the widths are larger than 10^{-5} a.u. The number of stable digits of the stationary eigenvalues is related to the Auger emission widths of the levels.

Physical properties display the same pattern as for antiprotonic helium [8]. A transition from atomic to molecular structure occurs between $L = 10$ and $L = 13$. For $L \leqslant 9$, the structure approximately consists in a double hydrogenlike system. The energies and mean distances between particles of excited states obtained for $L = 0 - 5$ display clear hydrogenlike properties. For $L \geqslant 13$, a pseudomolecular structure appears. Both atomlike and moleculelike structures are fairly described with the Born-Oppenheimer approximation.

For the sake of future experiments trying to measure the pion mass more precisely with techniques of atomic spectroscopy, we have studied the sensitivity of the energies to the value of the pion mass. Corrections of these energies for variations of this mass are presented.

The Lagrange-mesh method provides approximate wave functions in a simple analytical form with an accuracy close to the variational accuracy with the same basis. It allows analytical calculations of matrix elements for which the associated Gauss quadrature is not accurate enough. For example, they can be used to evaluate relativistic corrections and their pion mass dependence as we plan.

ACKNOWLEDGMENTS

This work was supported by the Fonds de la Recherche Scientifique–FNRS under Grant No. 4.45.10.08.

[1] T. Yamazaki, N. Morita, R. S. Hayano, E. Widmann, and J. Eades, Antiprotonic helium, Phys. Rep. **366**, 183 (2002).

[2] M. Hori, A. Dax, J. Eades, K. Gomikawa, R. S. Hayano, N. Ono, W. Pirkl, E. Widmann, H. A. Torii, B. Juhász, D. Barna, and D. Horváth, Determination of the Antiproton-to-Electron Mass Ratio by Precision Laser Spectroscopy of $\bar{p}\mathrm{He}^+$, Phys. Rev. Lett. **96**, 243401 (2006).

[3] M. Hori, H. Aghai-Khozani, A. Sótér, D. Barna, A. Dax, R. Hayano, T. Kobayashi, Y. Murakami, K. Todoroki, H. Yamada, D. Horváth, and L. Venturelli, Buffer-gas cooling of

antiprotonic helium to 1.5 to 1.7 K, and antiproton-to–electron mass ratio, Science **354**, 610 (2016).

[4] V. I. Korobov, D. Bakalov, and H. J. Monkhorst, Variational expansion for antiprotonic helium atoms, Phys. Rev. A **59**, R919 (1999).

[5] Y. Kino, H. Kudo, and M. Kamimura, High-precision Coulomb three-body calculation of antiprotonic helium atoms, Mod. Phys. Lett. A **18**, 388 (2003).

[6] V. I. Korobov, L. Hilico, and J.-P. Karr, Theoretical transition frequencies beyond 0.1 ppb accuracy in H_2^+, HD^+, and antiprotonic helium, Phys. Rev. A **89**, 032511 (2014).

[7] V. I. Korobov, L. Hilico, and J.-P. Karr, Bound-state QED calculations for antiprotonic helium, Hyperfine Interact. **233**, 75 (2015).

[8] D. Baye, J. Dohet-Eraly, and P. Schoofs, Structure changes along the lowest rotational band of the antiprotonic helium atom, Phys. Rev. A **99**, 022508 (2019).

[9] M. Hori, A. Sótér, and V. I. Korobov, Proposed method for laser spectroscopy of pionic helium atoms to determine the charged-pion mass, Phys. Rev. A **89**, 042515 (2014).

[10] M. Hori, H. Aghai-Khozani, A. Soter, A. Dax, and D. Barna, Laser spectroscopy of pionic helium atoms, Nature **581**, 37 (2020).

[11] G. T. Condo, On the absorption of negative pions by liquid helium, Phys. Lett. **9**, 65 (1964).

[12] J. E. Russell, Metastable States of $\alpha\pi^- e^-$, $\alpha K^- e^-$, and $\alpha\bar{p}e^-$ Atoms, Phys. Rev. Lett. **23**, 63 (1969).

[13] J. E. Russell, Structure of neutral mesonic atoms formed in liquid helium, Phys. Rev. A **1**, 721 (1970).

[14] J. E. Russell, Auger rates for circular orbits of $\alpha\pi^- e^-$, $\alpha\mathrm{K}^- e^-$, and $\alpha\bar{p}e^-$ atoms, Phys. Rev. A **1**, 742 (1970).

[15] J. Nuttall and H. L. Cohen, Method of complex coordinates for three-body calculations above the breakup threshold, Phys. Rev. **188**, 1542 (1969).

[16] Y. K. Ho, The method of complex coordinate rotation and its applications to atomic collision processes, Phys. Rep. **99**, 1 (1983).

[17] B. D. Obreshkov, V. I. Korobov, and D. D. Bakalov, Metastable states of the Condo type in exotic helium atoms, Phys. Rev. A **67**, 042502 (2003).

[18] D. Baye and P.-H. Heenen, Generalised meshes for quantum mechanical problems, J. Phys. A **19**, 2041 (1986).

[19] M. Vincke, L. Malegat, and D. Baye, Regularization of singularities in Lagrange-mesh calculations, J. Phys. B **26**, 811 (1993).

[20] D. Baye, M. Hesse, and M. Vincke, The unexplained accuracy of the Lagrange-mesh method, Phys. Rev. E **65**, 026701 (2002).

[21] M. Hesse and D. Baye, Lagrange-mesh calculations of three-body atoms and molecules, J. Phys. B **32**, 5605 (1999).

[22] M. Hesse and D. Baye, Lagrange-mesh calculations of the ground-state rotational bands of the H_2^+ and D_2^+ molecular ions, J. Phys. B **36**, 139 (2003).

[23] D. Baye, The Lagrange-mesh method, Phys. Rep. **565**, 1 (2015).

[24] A. S. Coolidge and H. M. James, On the convergence of the Hylleraas variational method, Phys. Rev. **51**, 855 (1937).

[25] C. L. Pekeris, Ground state of two-electron atoms, Phys. Rev. **112**, 1649 (1958).

[26] D. Baye and J. Dohet-Eraly, Quasibound states of an antiproton and a hydrogen atom, Phys. Rev. A **101**, 022507 (2020).

[27] M. Hesse and D. Baye, Lagrange-mesh calculations of excited states of three-body atoms and molecules, J. Phys. B **34**, 1425 (2001).

[28] M. Bollhöfer and Y. Notay, JADAMILU: A software code for computing selected eigenvalues of large sparse symmetric matrices, Comput. Phys. Commun. **177**, 951 (2007).

[29] E. Polizzi, Density-matrix-based algorithm for solving eigenvalue problems, Phys. Rev. B **79**, 115112 (2009).

[30] J. Kestyn, E. Polizzi, and P. T. P. Tang, FEAST eigensolver for non-Hermitian problems, SIAM J. Sci. Comput. **38**, S772 (2016).

[31] CODATA, CODATA 2018, http://physics.nist.gov/constants (2018).

[32] Particle Data Group *et al.*, Review of particle physics, Progr. Theor. Exp. Phys. **2020**, 083C01 (2020).

[33] V. I. Korobov, A. K. Bekbaev, D. T. Aznabayev, and S. A. Zhaugasheva, Polarizability of the pionic helium atom, J. Phys. B **48**, 245006 (2015).

[34] R. F. Wallis, R. Herman, and H. W. Milnes, Energy levels of an electron in the field of a finite dipole, J. Mol. Spectrosc. **4**, 51 (1960).

[35] M. Vincke and D. Baye, Hydrogen molecular ion in an aligned strong magnetic field by the Lagrange-mesh method, J. Phys. B **39**, 2605 (2006).